NANO · MICRO small
www.small-journal.com

Capillary-Scale Hydrogel Microchannel Networks by Wire Templating

*Shusei Kawara, Brian Cunningham, James Bezer, Neelima KC, Jingwen Zhu, Meng-Xing Tang, Jun Ishihara, James J. Choi, and Sam H. Au**

Microvascular networks are essential for the efficient transport of nutrients, waste products, and drugs throughout the body. Wire-templating is an accessible method for generating laboratory models of these blood vessel networks, but it has difficulty fabricating microchannels with diameters of ten microns and narrower, a requirement for modeling human capillaries. This study describes a suite of surface modification techniques to selectively control the interactions amongst wires, hydrogels, and world-to-chip interfaces. This wire templating method enables the fabrication of perfusable hydrogel-based rounded cross-section capillary-scale networks whose diameters controllably narrow at bifurcations down to 6.1 ± 0.3 microns in diameter. Due to its low cost, accessibility, and compatibility with a wide range of common hydrogels of tunable stiffnesses such as collagen, this technique may increase the fidelity of experimental models of capillary networks for the study of human health and disease.

1. Introduction

The microvasculature is a crucial component of tissues involved in transporting nutrients, wastes, drugs,[1] contrast agents for medical imaging,[2,3] as well as immune and metastatic cancer cells.[4] Laboratory models of the microvasculature are therefore valuable tools for studying human health and disease. Photolithography is commonly used to fabricate devices comprised of elastomeric polymers such as polydimethylsiloxane (PDMS) when dimensions and flow conditions need to be precisely controlled.[5] PDMS-based models, however, have a number of drawbacks. First, standard photolithography generates rectangular and not rounded cross-section microchannels.[6] Whilst post-processing can be used to fabricate rounded lumina,[7-9] the final diameters of these microchannels are often inconsistent and difficult to control. Second, typical PDMS devices are far stiffer (>800 kPa in Young's moduli) than human organs and vasculature.[10] Third, standard photolithography is limited to 2D planar geometries, requiring multilayer alignment or more elaborate techniques to construct 3D models.[11] Finally, though PDMS is gas permeable, it does not permit the migration, adhesion and survival of cells and other important biological elements, such as extracellular vesicles, drugs and nanoparticles within its matrix.[7]

A number of hydrogel-based models have been developed to overcome these limitations since hydrogels have superior biocompatibility and their mechanical stiffness can be tailored to match that of desired tissues.[12] Several groups have used "wire templating", where a hydrogel is cast around an extractable wire, to generate hydrogel-based microvasculature models. Wires of metal,[13–17] sacrificial sugars/polymers[6,18–20] and other elastic polymers[14,21–25] have been used to form hydrogel microchannels whose Young's moduli resemble those of tissues.[13] This method is simple, inexpensive, and has been deployed to generate microchannel lumens of diameters ranging from 10 to 1000 μm. Wire templating can achieve better resolutions than 3D printed methods,[26,27] and is far lower in cost and potentially more rapid than multi-photon polymer ablation techniques.[7]

However, wire-template methods for generating microvasculature models currently suffer from several technical hurdles: a) Perfusion into capillary-scale microchannels can induce leakage at world-to-chip interfaces due to the high hydrodynamic resistances inherent to small-diameter microchannels.[28,29] This is a non-trivial problem since the hydrodynamic resistance of round microchannels scales approximately to the inverse fourth power.[30] Thus, narrowing a 250 μm diameter microchannel to 10 μm increases its theoretical hydrodynamic resistance by >390 000 fold, which can compromise model integrity when perfusion is attempted. While there are some existing methods to firmly couple syringes to hydrogel microchannels via needles,[13,21] luer-locks,[31] or bulb-shaped connectors,[32] these methods have only been demonstrated for large diameters (>250 μm) or require the use of non-hydrogel materials such as glass and PDMS in the vicinity of the microvasculature model which does not exhibit tissue-level mechanical stiffnesses.[9]

S. Kawara, B. Cunningham, J. Bezer, N. KC, J. Zhu, M.-X. Tang, J. Ishihara, J. J. Choi, S. H. Au
Department of Bioengineering
Imperial College London
South Kensington, London SW7 2AZ, UK
E-mail: s.au@imperial.ac.uk
B. Cunningham, S. H. Au
Cancer Research UK Convergence Science Centre
London SW7 2AZ, UK

The ORCID identification number(s) for the author(s) of this article can be found under https://doi.org/10.1002/smll.202301163

DOI: 10.1002/smll.202301163

Table 1. Comparison of recent wire templating methods for manufacturing microvasculature models in hydrogels. Mesh networks are comprised of microchannels that intersect in grid-like patterns while progressively narrowing bifurcations split in more physiological Y-shaped junctions.

Publication	Template wire material	Hydrogel (Concentration and Young's moduli [YM] if known)	Microchannel diameters	Round cross-section [Y/N]	Mesh networks [Y/N]	Progressively narrowing bifurcation [Y/N]	Multiple level bifurcations [Y/N]
X. Y. Wang et al., Lab Chip 2014[6]	Alginate[6]	Gelatine (12.5%, w/w) (YM < 20kPa[45]), agarose (1.0%, w/w) (YM ≈38 kPa[46]) and collagen (2.5 mg mL^{-1}) (YM > 100 kPa[47])	20–500 μm	N	Y	Y	Y
J. H. Bezer, et al., Ultrasound Med. Biol., 2020[13]	Metal [13]	Polyacrylamide (Acrylamide:Bis- = 4:0.1, 5:0.15, and 5:0.3 (%)) (YM = 2–8.7 kPa)	25–100 μm	Y	N	N	N
J. Lee et al., Tissue Eng. Regen. Med. 2018 [14]	Metal [14]	Acrylate hyaluronic acid (3%, 200 kDa, YM = 70–200 kPa[48,49] a))	500–600 μm	Y	N	N	N
S. Ma et al., Chem. Mater. 2018 [15]	Iron [15]	Various synthetic gel	>1000 μm	Y	Y	N	N
K. Yan et al., Soft Matter 2020[16]	Metal[16]	Chitosan (1.0 w/v%, 220 kDa, deacetylation of 85%, YM <5 MPa[50] b))	400 μm	Y	N	N	N
X. Zhao et al., Ultrason. Sonochem. 2023[17]	Metal[17]	Agar (2.5%, YM ≈254 kPa[46] c))	2000–15 μm	Y	N	N	N
J. S. Miller et al., Nat. Mater. 2012[18]	Carbohydrate-glass[18]	Poly(ethylene glycol) diacrylate (5, 10, or 20%, 6 or 35 kDa), acrylate-PEG-RGDS (1 mM, 4 kDa), Fibrin gels (10–40 mg mL^{-1}), Matrigel, Alginate (2%)	>150 μm	Y	Y	Y	Y
M. Ryma et al., Adv. Mater. 2022[19]	poly(2-cyclopropyl-2-oxazoline) [19]	GelMA (3.08–34.9 kPa[51] d))	>220 μm	Y	N	Y	Y
L. E. Bertassoniet al., Lab Chip 2014[21]	Agarose[21]	GelMA (10% 3.08–34.9 kPa[51] d))/PEGDA/PEGDMA/SPELA	>150 μm	Y	Y	Y	N
N. Zhao et al., Adv. Funct. Mater. 2022[22]	Polymer fibre[22]	Agarose (2%,≈50 kPa[52] e))	10 μm	Y	Y	N	N
J. Nie et al., Mater. Horizons 2020[23]	Polymer fibre[23]	Gelatine/GelMA (10%)	200–800 μm	Y	Y	Y	Y
T. C. Tseng et al., Biomaterials 2017[24]	Sacrificial gel[24]	Fibrin, chitosan	≈2500 μm	Y	N	N/A	Y
H. Yoshida et al., Adv. Funct. Mater. 2013[24]	Silica[24]	γ -PGA-SS hydrogels (2.0 mmol)	150–660 μm	Y	N	N	N
V. K. Lee et al., Biomaterials 2014[25]	Gelatine	Collagen (3 mg mL^{-1})	>500 μm	N/A	N	N	N
Kawara S. et al.	Metal (this study)	Polyacrylamide (Acrylamide:Bis- = 4:0.3, 3–4 kPa[40] f))GelMA(10%)/gelatine(gelatine (10%)/collagen-alginate(1.5 mg mL^{-1}, 10 mg mL^{-1})	>6.1 μm	Y	Y	Y	Y

[a–f)] Estimated values from the concentration of gels.

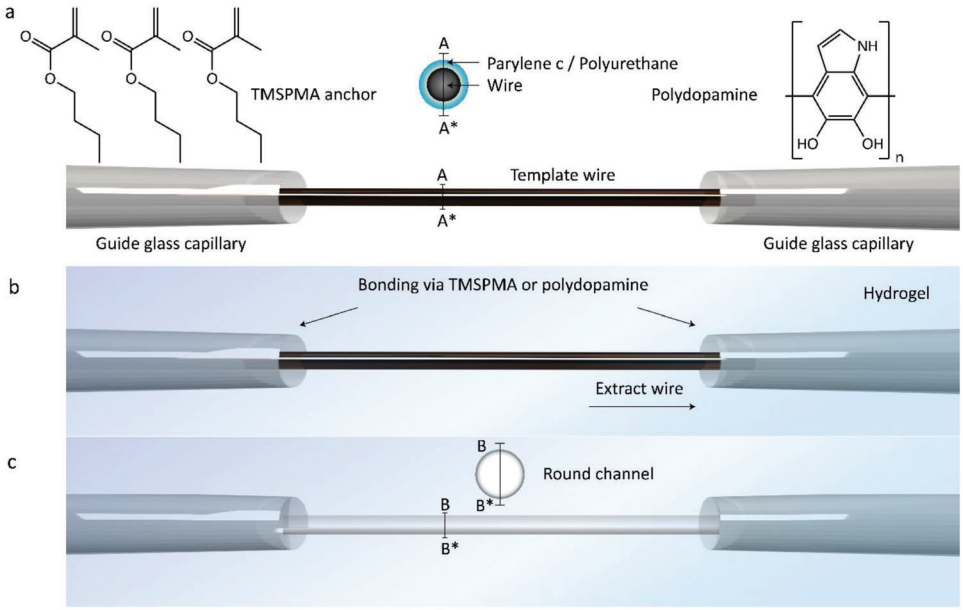

Figure 1. Surface modifications to create robust world-to-chip interfaces with various hydrogels. a) Guide glass capillaries treated with TMSPMA or polydopamine and loaded on alignment rig (see Figures S15–S19, Supporting Information). Parylene-c or polyurethane-coated template wire was inserted all the way from one guide glass capillary to another. b) Hydrogel precursor was polymerized in situ and formed a bond with the guide glass capillary that creates tightly sealed world-to-chip interfaces. c) The template wire was extracted to form a round cross-section microchannel.

b) The extraction of template wires often leads to non-uniformity and damage to hydrogels.[16] c) Wire templating has difficulty mimicking the geometry of human microvasculature networks that fractally branch into progressively narrower diameter channels at bifurcations.[13–16] Simple "Y-shaped" bifurcations in PDMS have been generated using wire templating.[31] But more physiological branching in hydrogels that controllably narrow at bifurcations has so far required either expensive multi-photon ablation equipment[7] or sacrificial scaffolds[6,18–25] that require specialized melt electrowriting capabilities and cannot print at capillary scale. Although single channels and mesh-like networks with diameters of 10–15 μm have been achieved with wire-templating, multi-order progressively narrowing bifurcations in hydrogels have yet to be reported at ≈5–10 micron human capillary scale (**Table 1**).

In this paper, we present a series of accessible techniques to fabricate capillary-scale models of human microvasculature. Our models feature fully-perfusable rounded cross-section multi-branching microchannel networks that reproducibly generate tightly-sealed inlets/outlets, with uniform, smooth and controllable inner diameters that can bifurcate and narrow fractally. Our techniques involve four key components: chemically-treated guide glass capillaries as world-to-chip interfaces, physical coating of wires to generate smooth microchannel lumens, surface tension-driven wire bundling to generate bifurcating wires, and 3D printed/laser-cut alignment rigs to control network geometries and facilitate perfusion.

2. Results

We encountered numerous obstacles in our early attempts to generate capillary-scale microchannel hydrogel networks. These included: leakage at world-to-chip interfaces, gel tearing during wire extraction, generation of wire-templated bifurcations, and perfusion of cells through bifurcating channels. We describe the experimental approaches we developed to solve each of these hurdles in turn. These include novel applications of surface modification techniques to seal interfaces (**Figure 1**) and dip coating to generate wire bifurcations (**Figure 2**).

2.1. Surface Chemistry Solves Leakiness of the World-To-Chip Interface

Commercial borosilicate glass capillaries are excellent supporting "guides" for wire-templating in hydrogels because of their biocompatibility, autoclavability, uniformity, optical transparency, compatibility with flexible laboratory tubing, and linearity (which assists in the alignment of microchannels after wire extraction). However, in our initial attempts at microchannel formation, we noticed the poor adhesion of hydrogels to the guide glass capillaries (**Figure 3**a). This caused the collapse and deformation of the glass-gel interface and the expulsion of gel once hydrostatic pressure was applied. Even at pressures as low as 100 mm H_2O, FITC-dextran solution leaked through the gap between the glass capillary and gel (Figure 3a), preventing perfusion through the microchannels.

To overcome leakage in the gel-glass interface, we chemically modified borosilicate guide glass capillaries with either 3-(trimethoxysilyl) propyl methacrylate (TMSPMA) or polydopamine prior to gel casting. TMSPMA initiated covalent bonding between silicon in glass and acrylate groups in hydrogels such as polyacrylamide[33] while polydopamine promoted adhesion between organic and inorganic surfaces,[34] making this method

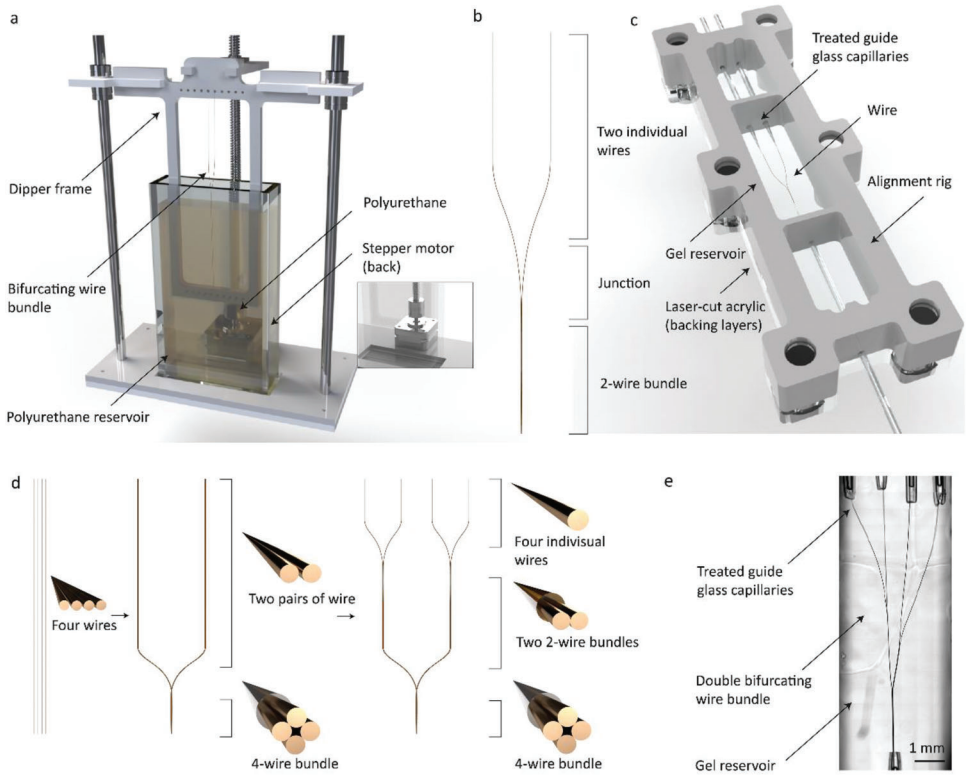

Figure 2. Manufacturing of bifurcating microchannel networks. a) Overview of dipper rig. Wire-loaded frame is driven up and down by Arduino-controlled stepper motor to dip coat wires in polyurethane reservoir. b) Schematic of single bifurcating wire bundles. c) Schematic of single bifurcating wire bundle loaded on the alignment rig. d) Schematic of double bifurcating wire bundles.e) Photograph of double bifurcating wire bundle loaded on the alignment rig.

compatible with most hydrogels on the market (Figure 1a).[35] Guide glass capillaries treated in these manners led to interfaces that remained intact even under ramping pressures up to 500 mm H_2O (greater than physiological capillary pressure in humans of ≈140–300 mm H_2O[36]). These microchannels operated without leakage of FITC-dextran or rupture along their 30 mm lengths (Figure 3a), and importantly permitted consistent and reliable perfusion. To further test for leakage, we then compared the volumetric flow rate at each hydrostatic pressure value to theoretically derived values (Figure 3b). Experimental values showed good agreement with theoretical for both hydrostatic pressure-driven and syringe pump-driven experiments. There was no statistically significant difference between experimental and theoretical rates ($p > 0.05$) except for small discrepancies at the lowest tested pressures of 100 at 200 mm H_2O.

To further test the robustness of the guide capillary-hydrogel interface, we subjected microchannels to ramping FITC-dextran flows from 0.01 μL s^{-1} to 1 μL s^{-1} (corresponding to pressure drops up to ≈400 mm H_20). Microchannels fabricated with TMPSMA- or polydopamine-treated guide glass capillaries showed microchannel deformations more similar to theoretical values when we assumed no loss of fluid than untreated guide capillaries (Figure 3c). Leakage in all untreated capillaries resulted in inconsistent flow rates among experimental replicates, as demonstrated by large deviations in data points (Figure 3c).

2.2. Physical Modification of Wires Surfaces Prevents Hydrogel Damage During Wire Extraction

The extraction of template wires can lead to tearing and damage to microchannel walls due to friction forces between wire surfaces and casted hydrogels as shown in **Figure 4**. To overcome this, we coated template wires with either parylene-c by vapor deposition or polyurethane by dip coating (Figure 1b,c). These methods improved microchannel uniformity and structure likely due to the low roughness and hydrophobic nature of these coatings (Figure 4a).[37] We also found that the smoothness and regularity of microchannel lumens were largely influenced by the straightness of template wires and speed of extraction; with straight wires and low extraction rates producing higher quality microchannels (data not shown).

After deploying the chemical and physical surface modification strategies described above, single microchannels fabricated in polyacrylamide, gelatine, and gelatine methacrylate (GelMA) were flushed with 2000 kDa FITC-dextran solution (Figure 4b–f). TMSPMA-treated guide capillaries were used for polyacrylamide and GelMA hydrogels while polydopamine-treated guide capillaries were used for natural hydrogels. The resulting microchannels had smooth regular surfaces without rupture across their full 30 mm lengths. Cross-sectional images of the channel in polyacrylamide confirmed that round cross-section microchannels were generated with this wire-templating method using 100, 10, and 5 μm cross-sectional nominal

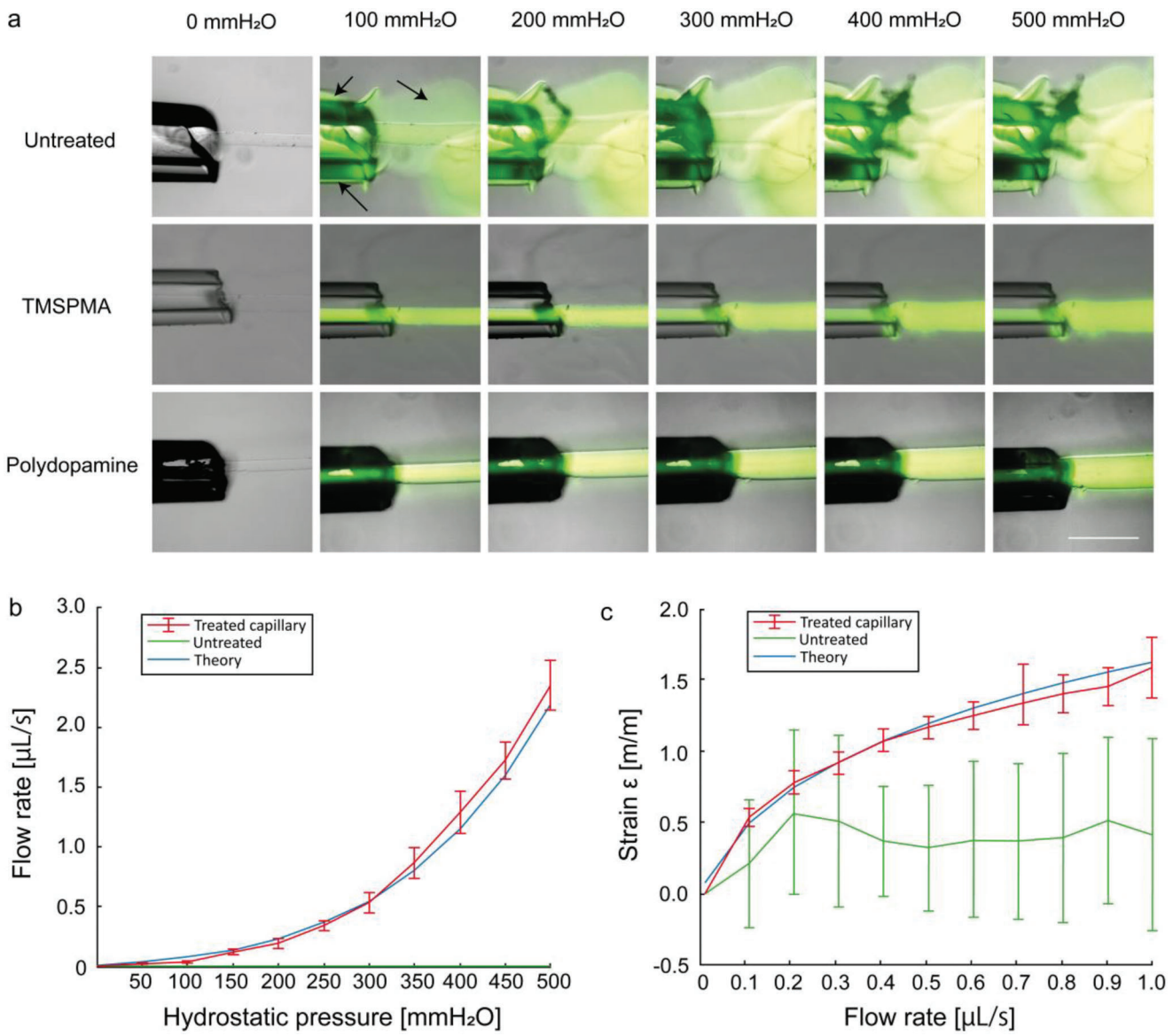

Figure 3. Development of robust World-to-Chip Interface. a) Representative images of guide capillary-microchannel interfaces under infused hydrostatic pressures from 0 to 500 mm H_2O of FITC-dextran (2000 kDa molecular weight) either untreated or treated with TMSPMA or polydopamine. Black Arrows indicate leakage of the FITC-dextran solution. b) Correlation of hydrostatic pressure to flow rate in the channel. c) Normalized deformation in TMSPMA/polydopamine treated or untreated capillaries versus theoretical deformation at flow rates from 0 to 1 µL min^{-1}. Error bar represents one SD, $n = 9$, Scale bar: 500 µm.

diameters (Figure 4b–d). The resulting channel diameters, measured at multiple points along each microchannel, were 113.9 ± 2, 10.5 ± 0.2, and 6.1 ± 0.3 µm, respectively. Manufacturer tolerances in template wires and the addition of surface coatings most likely led to the discrepancies between nominal and measured diameters.

2.3. Polyurethane Dip Coating Generates Progressively Narrowing Bifurcating Template Wire Bundles

To mimic the fractal bifurcations present in human capillaries geometries, we used surface tension to selectively merge template wires into bundles (Figure 2). We first developed an Arduino-controlled low-cost 3D printed/laser-cut "dipper rig" (Figure 2a) to automate the dip coating of template wires and a 3D printed/laser-cut "alignment rig" (Figure 2c) for hydrogel casting and perfusion. Comprehensive instructions for replicating both the dipper and alignment rigs are freely available in the electronic supplementary material. By partially submerging and extracting hung wires from a bath of polyurethane in the dipper rig, we could induce wires to irreversibly merge (Movie S2, Supporting Information). This generated bifurcations along the lengths of the template wires, the location of which could be simply controlled by setting the dip height. Two added advantages of polyurethane dip coating were that the template

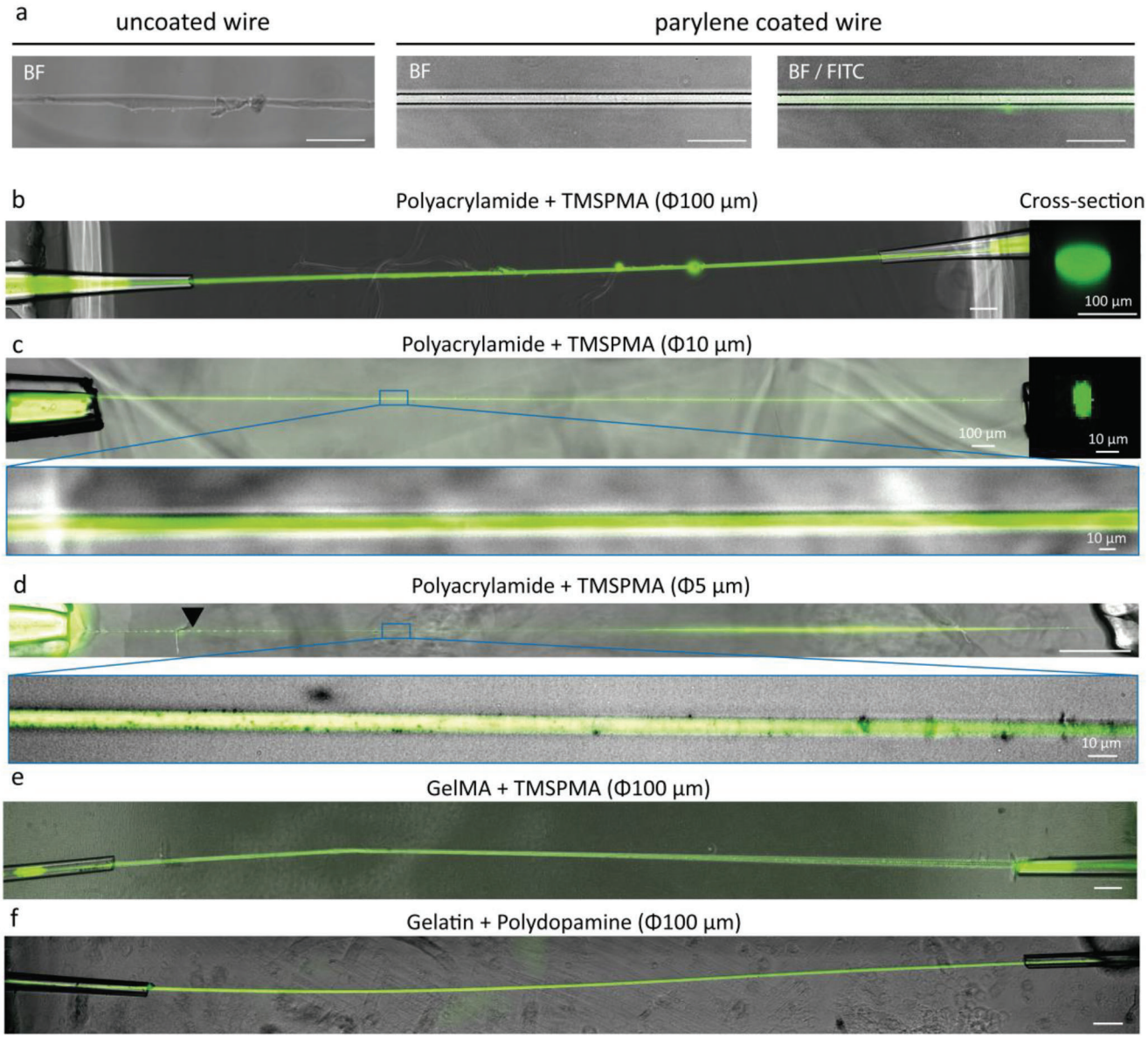

Figure 4. Single microchannels in various hydrogels. a) Comparison of parylene-c-coated versus uncoated copper wire as a template in 10 µm nominal diameter microchannel in brightfield (BF) or merged with green fluorescence using FITC-dextran (2000 kDa MW solution) (BF/FITC). b) Photomicrograph of 100 µm nominal diameter microchannel in polyacrylamide with cross-section image (right). c) Merged image of 10 µm nominal diameter – microchannel with polyacrylamide/TMSPMA with a cross-section (right). d) Merged image of 5 µm nominal diameter – microchannel with polyacrylamide/TMSPMA. Arrows indicate polyurethane beading generated to improve the handling of narrow diameter template wires (see supporting information for details). e) Photomicrograph of 100 µm nominal diameter microchannel with GelMA/TMSPMA. f) Photomicrograph of 100 µm nominal diameter microchannel with gelatine/polydopamine. Unless otherwise specified, scale bar: 500 µm.

wires did not need to be further modified by parylene-c or other coatings before application, and the dip coating bonded the wires with enough strength to withstand wire template extraction (0.41 ± 0.06 Nwas required to separate 100 µm diameter template wires after 20 dips) (Figure S12, Supporting Information). As a demonstration, we generated "single bifurcation" microchannels generated by merging two 10 µm (**Figure 5**a,b) or two 100 µm (Figure S1, Supporting Information) nominal diameter wires into one bundle; and "double bifurcations" networks generated by merging four 20 µm nominal diameter wires into two and then one bundle either with fewer (Figure 5c) or greater (Figure S2, Supporting Information) numbers of programmed polyurethane dip cycles (see supplementary methods for details). Bifurcating daughter microchannels generated in this manner narrowed at bifurcations with cross-sectional diameters of respective parental and daughter microchannels of 21.4 ± 1 and 10.1 ± 0.2/10.3 ± 0.4 µm for 10 µm nominal diameter single bifurcations (Figure 5b) and 223.7 ± 7 and 110.1 ± 4/105.6 ± 1 µm for 100 µm nominal diameter single bifurcations (Figure S1, Supporting Information). For double

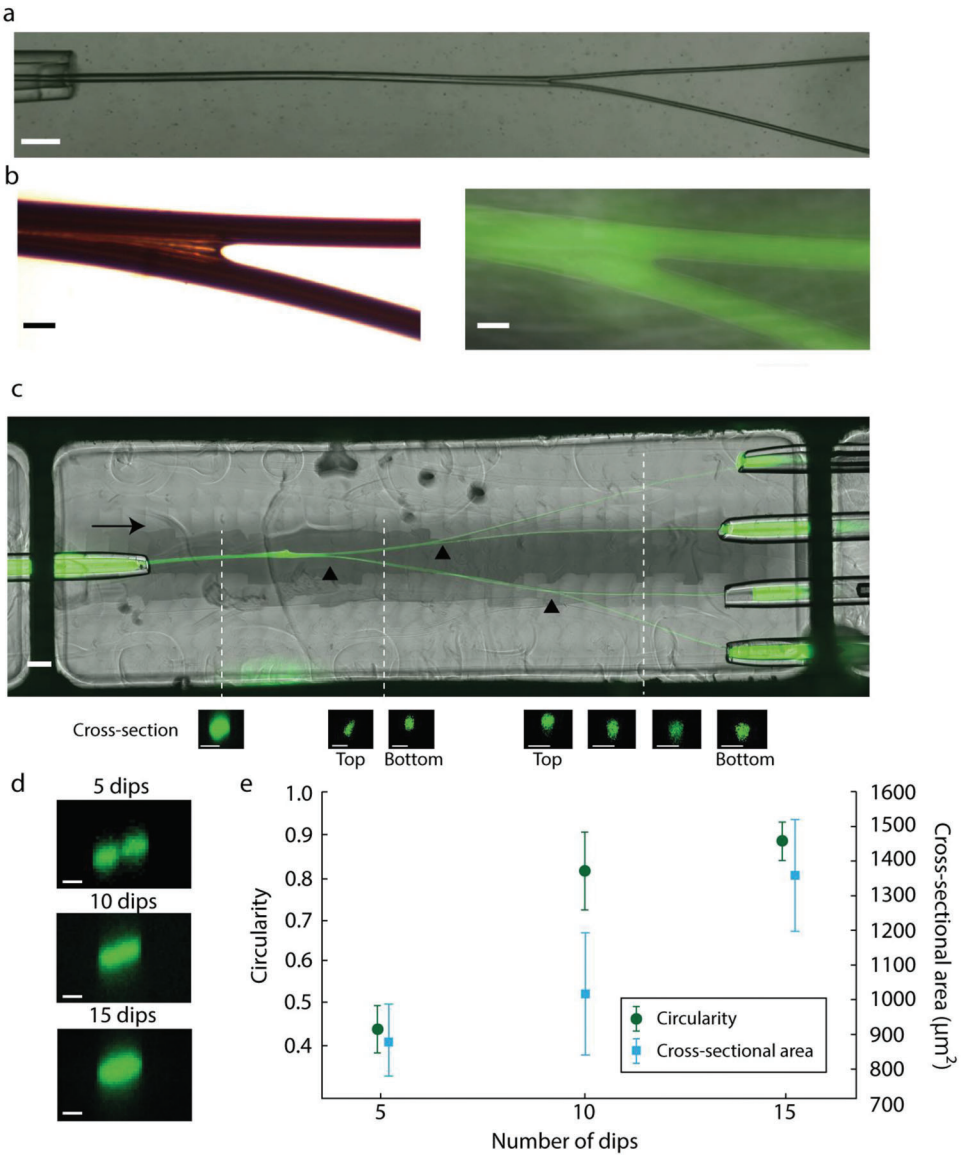

Figure 5. Bifurcating microchannels brightfield and after infusion with FITC-dextran. a) Symmetrical single bifurcation made using 10 μm nominal diameter template wires in collagen. Scale bar: 500 μm. b) Asymmetrical bifurcation made using 10 μm nominal diameter template wires in polyacrylamide; wire template (left) and resulting channel (right). Scale bar: 10 μm. c) Double bifurcating networks were made using 20 μm nominal diameter template wires in polyacrylamide with confocal cross-sectional images (Scale bar:100 μm for truncal (left) and first order (middle) microchannels, and 50 μm second order microchannels (right). Arrow indicates the direction of flow and arrowheads indicate bifurcations. Scale bar in main image: 1 mm. d) Cross-section of channel generated after respective numbers of automated dip cycles of 10 μm diameter wires in polyurethane. e) Cross-sectional circularity (circle dots, left) and cross-sectional area (square dots, right) of microchannels fabricated from 10 μm nominal diameter wires after 5, 10, and 15 dips in polyurethane, error bars represent standard deviation, $n = 9$. Scale bar: 10 μm.

bifurcations using 20 μm nominal diameter wires, cross-sectional diameters of respective parental,daughter and granddaughter microchannels were measured as 99.1 ± 4, 58.9 ± 11/59.0 ± 2 and 29.6 ± 2/32.0 ± 0.8/34.5 ± 4/32.2 ± 1.4 μm when fabricated using fewer number of dip cycles (Figure S13, Supporting Information for fabrication details) (Figure 5c). When wires were dipped with a greater number of dip cycles, cross-sectional diameters of respective parental and daughter and granddaughter microchannels were measured as 302.4 ± 4 , 126.2 ± 14/116.8 ± 17 and 38.0 ± 3/47.2 ± 6/35.6 ± 5/38.4 ± 5 μm (Figure S2, Supporting Information). The non-uniform profile of the channels was most likely due to Rayleigh-Plateu instability when excessive amounts of polyurethane were over-deposited onto wire bundles. To mimic symmetrical and asymmetrical bifurcation of true blood vessels, we adjusted the positions of guide glass capillaries and template wires in the alignment rig, to generate both symmetrical (Figure 5c (top)) and asymmetrical bifurcations (Figure 5c (bottom)) using our technique. We also conducted confocal microscopy on FITC-dextran perfused single bifurcations to measure the circularity of microchannel

cross-sections (Figure 5d,e). We noticed increasing levels of lumen circularity as we increased the number of dip cycles with circularity values of 0.45 ± 0.12 after five dips up to 0.88 ± 0.04 after 15 or more dips. We noticed that dip coating >15 times often led to the formation of beads of polyurethane due to Plateau-Rayleigh instability[38] that is commonly seen when circularity approaches one (Figure S14d, Supporting Information).

2.4. Incorporation of Cellular Elements

To study the compatibility of our hydrogel-based wire-templating systems with living cells, we introduced both tumor cells (to explore their transit) and endothelial cells (to investigate their adhesion as a component of the vascular endothelium). B16-OVA melanoma cancer cells were infused into symmetrical single bifurcation microchannels with parent and daughter branch diameters of ≈20.9 and 13.0/12.4 µm, respectively (Figure S3, Supporting Information). Tumor cells presented with a mean diameter of 9.2 µm with a range of 7.2–11.0 µm (Figure S3b, Supporting Information). Cells transited successfully through the bifurcations (Movie S1, Supporting Information). Interestingly, similar to true microvasculature, the microchannels changed in diameter in response to flow. Parent and daughter branches increased in diameter by ≈31% and 12%, respectively, in response to 0.01 µL sec^{-1} volumetric flow rate when compared to static conditions (expansions of up to ≈50% have been observed in true blood vessels[39]). This degree of microchannel expansion is not observed in PDMS-based devices and is likely a result of the fact that our channels are closer to tissue stiffness (polyacrylamide Young's Modulus = ≈3.24 ± 0.58 kPa[40]). Primarily endothelial cells were also successfully attached to the inner lumen of ≈200 µm diameter single channels (Figure S4, Supporting Information) and bifurcations after 24 h of incubation. Cells remained attached to the walls of our hydrogel lumen and calcein-AM viability stains indicated that the cells remained alive.

2.5. Super-Resolution Imaging Using Ultrasound Contrast Agents

We explored whether our platform could be used for ultrasound contrast imaging. To do this we perfused lipid-shell gas-core microbubbles into "wall-less" 10 and 100 µm nominal diameter microchannels of 4% acrylamide and 0.3% bis-acrylamide (expected Young's modulus is ≈3.24 ± 0.58 kPa[40]). Ultrasound contrast agents were infused successfully without any leakage (Movie S4, Supporting Information), which is significant for imaging purposes as leakage of contrast agents around the vicinity of the ultrasound beam leads to misinterpretation of acquired acoustic data, a common problem in the field. Contrast-agent enhanced super-resolution images were then successfully acquired from 100 µm nominal diameter microchannels (Figure S21, Supporting Information), indicating that our microvasculature models are compatible with ultrasound imaging due to the matching acoustic properties of our phantom.

3. Discussion

In this paper, we demonstrate how the combination of chemical surface modifications, physical surface modifications, and surface-tension-driven wire bundling can be deployed to generate hydrogel microvasculature models by wire templating. These models feature up to two sequential and progressively narrowing bifurcating branches with control over lumen diameters down to 6.1 µm in various hydrogels including collagen. To our knowledge, this is the first report of any wire templating method to generate true capillary scale microchannel bifurcations and the first report of a wire templating method that mimics the progressively narrowing fractal nature at the microvasculature scale.

Importantly, we designed our method to be both accessible and inexpensive. All necessary computer-assisted design files and component lists (Table S1, Supporting Information) are available to download from the electronic supporting information. The Components were chosen to be widely available and as cost-effective as possible. At the time of writing, we estimate that equipment costs, including Arduino-controlled automated dipper rigs, and alignment rigs to be ≈140 USD (Tables S1–S3, Supporting Information), and the cost of consumables (template wires, guide glass capillaries, and polyacrylamide hydrogel) equal to ≈10 USD per device (Table S4, Supporting Information). This is significantly lower in cost than the only other available technique for generating controlled capillary-scale networks in hydrogels, multiphoton laser ablation, whose commercial costs are often in excess of 500 000 USD.

Our wire templating technique does have some limitations. First, handling capillary-scale template wires can often be difficult because of their size and fragility. We found that magnifying lenses assisted in the handling of 5 and 10 µm diameter wires and selective dip coating of inlet portions of 5 µm diameter wires (see supplementary methods) helpful. Second, while we achieved good control over the diameters of single straight microchannels (Figures 3–4) (e.g., by choosing template wires and amount of parylene c to deposit), we did not have full control over the dimensions of bifurcating microchannels. There appears to be a non-linear relationship between the number of dip cycles and final dimensions for the double bifurcations networks (Figure 5c; Figure S2, Supporting Information). We noticed that polyurethane thickness, as influenced by the number of template wire dip cycles, could alter the ratios of parent and daughter branches. More work needs to be done to explore if this strategy, amongst others, may provide users with precise control over bifurcation geometries, for instance to better approximate Murray's Law. It should be noted however, that accurate models of capillary scale bifurcations may not obey Murray's Law[41] due to the influence of formed elements that may result in turbulent[42] and non-Newtonian[41,43,44] blood flows. Furthermore, because of the vertical nature of our dipping rig, we have not been able to fabricate wire templates that both progressively branch and converge to mimic both the arterial and venous components of microvasculature in a single device. We have however connected two separate bifurcating devices with external tubing in a "mirrored" configuration (Figure S5, Supporting Information) that may be expanded in future studies to build a complete microvasculature model.

We foresee many potential applications for this technique such as studies on the metastasis and invasion of circulating tumor cells, drug delivery and cardiovascular disease. Furthermore, because hydrogels have acoustic properties more closely aligned to water, our microvascular model is compatible with in vitro

studies of acoustic cavitations of ultrasound contrast agents for imaging and therapy.

4. Conclusion

This study presents a suite of techniques to fabricate perfusable capillary-sized, round cross-section microchannels in hydrogel by wire templating. Both straight channel and bifurcating geometries, as well as endothelial cell coating were demonstrated in this study. This technique is accessible, low cost and suitable for a variety of optically transparent acrylate-based hydrogels (e.g., polyacrylamide, gelatine methacrylate) as well as mammalian hydrogels (e.g., collagen, alginate, gelatine, and matrigel). These techniques may be valuable for studies in the many areas of human health and disease where microvasculature models are desired.

5. Experimental Section

Microfabrication Methodology: Microchannels were fabricated by wire-templating involving three phases (Figure S6, Supporting Information): 1) surface-treatment of guide glass capillaries (Figure S7, Supporting Information), 2) template wire coating (Figures S8–S14, Supporting Information), and 3) assembly and channel formation (Figures S15–S20, Supporting Information). Wire-templated single microchannels were fabricated with TMSPMA/polydopamine-treated guide glass capillaries, custom alignment rigs and parylene-c- or polyurethane-coated wires. Fabrication of bifurcating channels required additional steps to generate bifurcating wire bundles by dip coating of polyurethane with a custom dipper rig. Rig components were laser-cut (Fusion Pro 36, Epilog Laser, UK) and 3D printed (Markforged Onyx Pro, Markforged, UK), as necessary. Detailed methods can be found in the supporting information alongside step-by-step visual instructions (Figures S7–S20, Supporting Information) and component lists (Tables S1–S4, Supporting Information).

Microchannel Perfusion: To test the robustness of the channel, 2.5 mg mL^{-1} of fluorescein isothiocyanate (FITC) – dextran (2000 kDa) (Sigma-Aldrich, UK) in DI water was infused into microchannels through silicone tubing (STHT-C-030-0, 1.676 mm OD, 0.762 mm ID, Cole-Palmer, UK) connected to the guide glass capillary inlet. Microchannels were either perfused by pressure control via hydrostatic head or flow rate control via syringe pump as described below. All the images including single and stitched images (30% overlap, manual focus points with linear interpolation) were taken with bright field and fluorescent microscopy (Nikon Ti-2 E, Nikon, UK) and a confocal microscope (Leica SP8, Leica, Germany).

For pressure control, the infusion pressure was controlled and ramped up by hydrostatic pressure from 0 mm H_2O to 500 mm H2O by increasing the head height of the solution. Flow rates were calculated by collecting five parts of solution passed through the channel over one minute. Theoretical flow rates (m^3 s − 1) were generated as a function of pressure drop according to:

$$\Delta P = \sum_{k=1}^{n} \frac{128\mu q\,(l/n)}{\pi d_k^4} \tag{1}$$

where $d_k = d_o \left(\left(\sum_{m=1}^{k} \frac{128\mu q(l/n)}{\pi d_m^2} \right) / E + 1 \right)$, ΔP is the overall pressure drop in the channel, μ is the dynamic viscosity of fluid (1.0×10^{-3} Pa s), q is volumetric flow rate (m^3 s1), l is the length of the channel (0.03 m), n is a finite number of slices in the longitudinal distance of the channel (>10 000), d_o is an initial diameter of the channel (100 μm), d_k is a diameter of a deformed channel at point k ($1 \le k \le n$) in the channel, d_m is a diameter of a deformed channel at point m ($1 \le m \le k$)) in the channel, and E is Young's modulus of polyacrylamide gel (≈3.24 ± 0.58 kPa[40]).

For flow rate control, the flow of 2.5 mg mL^{-1} 2000 kDa-FITC-dextran dissolved in DI water was increased linearly from 0.01 to 1 μL s^{-1} using a 1 mL syringe (Fisher Scientific, UK) controlled by a syringe pump (PHD Ultra, Harvard Apparatus, Holliston, MA, USA) over 30 min. Five measurements of deformation were taken. The theoretical curve for channel deformation at the inlet was generated by calculating the pressure drop in the channel based on the deformation of the channel wall using Equation (1). Images of the channel were taken with fluorescence microscopy.

Characterizing Circularity and Cross-Sectional of Bifurcating Microchannel: Single bifurcating wire bundles were made with 10 μm nominal diameter wires and microchannels were formed as described above. Three numbers of dip were selected; 5, 10, and 15 and the experiment was conducted in triplicate. 2.5 mg mL^{-1} of fluorescein isothiocyanate (FITC) – dextran (2000 kDa) (Sigma–Aldrich, UK) in DI water solution was infused into a single microchannel through silicone tubing connected to the guide glass capillary inlet. Cross-sectional images were then taken for three selected points for each channel by confocal microscopy ($n = 3 \times 3$). Circularity (c) was then examined through FIJI software based on $c = 4\pi\ (A/P2)$, where c is non-dimensional circularity ($0 < c < 1$), A is area (m^2) and P is perimeter (m). Cross-sectional area for each number of dips was also measured using the cross-sectional images through FIJI software.

Statistical Analysis: Pre-processing of data, data presentation and sample sizes are stated in each experimental subsection. Student's t-tests were used to calculate the difference between means, with p-values <0.05 considered significant. Data are presented as means and errors are presented as one standard deviation (SD) unless stated otherwise. All statistical analysis was carried out with MATLAB software (ver. 2021b, MathWorks, US).

Supporting Information

Supporting Information is available from the Wiley Online Library or from the author.

Acknowledgements

This research project was funded/supported by the Rotary International Global Grant (GG2014756), JASSO Postgraduate Scholarship (G2299999919N), Cancer Research UK (DRCMDPA\100008), the CRUK Convergence Science Centre at The Institute of Cancer Research, London, and Imperial College London (A26234), and EPSRC CDT EP/L015226/1, China Scholarship Council, and EPSRC under Grant EP/T008970/1. This work utilized expertise and prototyping equipment at the Imperial College Advanced Hackspace. The authors also thank Florent Seichepine for assisting vapor deposition process and William Lim Kee Chang for providing his expertise in chemistry. [Correction added after publication 18 October 2023: Table 1 was corrected.]

Conflict of Interest

The authors declare no conflict of interest.

Author Contributions

S.K. and B.C. contributed equally to this work. S.K. contributed to the overall manufacturing of wire-templated single channels and manuscript preparation. B.C. contributed to the generation of bifurcations and manuscript preparation. J.B. provided the first idea of wire templating. N.KC. helped in incorporating cellular in hydrogel channel. and J.Z. helped in ultrasound imaging. M-X.T., J.I., J.J.C. and S.H.A. were responsible for idea generation, supervision, and manuscript writing. All authors contributed to edits.

Data Availability Statement

The data that support the findings of this study are available from the corresponding author upon reasonable request.

Keywords

bifurcations, capillaries, hydrogel, microchannels, microvasculature, phantom, wire-templating

Received: February 9, 2023
Revised: April 8, 2023
Published online: June 2, 2023

[1] S. Azzi, J. K. Hebda, J. Gavard, *Front. Oncol.* **2013**, *3*, 211.
[2] K. Christensen-Jeffries, O. Couture, P. A. Dayton, Y. C. Eldar, K. Hynynen, F. Kiessling, M. O'Reilly, G. F. Pinton, G. Schmitz, M. X. Tang, M. Tanter, R. J. G. van Sloun, *Ultrasound Med. Biol.* **2020**, *46*, 865.
[3] M. Versluis, E. Stride, G. Lajoinie, B. Dollet, T. Segers, *Ultrasound Med. Biol.* **2020**, *46*, 2117.
[4] J. Perea Paizal, S. H. Au, C. Bakal, *Br. J. Cancer* **2021**, *124*, 58.
[5] S. H. Au, B. D. Storey, J. C. Moore, Q. Tang, Y. L. Chen, S. Javaid, A. F. Sarioglu, R. Sullivan, M. W. Madden, R. O'Keefe, D. A. Haber, S. Maheswaran, D. M. Langenau, S. L. Stott, M. Toner, *Proc. Natl. Acad. Sci. U. S. A.* **2016**, *113*, 4947.
[6] X. Y. Wang, Z. H. Jin, B. W. Gan, S. W. Lv, M. Xie, W. H. Huang, *Lab Chip* **2014**, *14*, 2709.
[7] C. Arakawa, C. Gunnarsson, C. Howard, M. Bernabeu, K. Phong, E. Yang, C. A. DeForest, J. D. Smith, Y. Zheng, *Sci. Adv.* **2020**, *6*, eaay7243.
[8] M. Abdelgawad, C. Wu, W. Y. Chien, W. R. Geddie, M. A. S. Jewett, Y. Sun, *Lab Chip* **2011**, *11*, 545.
[9] L. K. Fiddes, N. Raz, S. Srigunapalan, E. Tumarkan, C. A. Simmons, A. R. Wheeler, E. Kumacheva, *Biomaterials* **2010**, *31*, 3459.
[10] R. Seghir, S. Arscott, *Sens. Actuators, A* **2015**, *230*, 33.
[11] H. Luan, Q. Zhang, T. L. Liu, X. Wang, S. Zhao, H. Wang, S. Yao, Y. Xue, J. W. Kwak, W. Bai, Y. Xu, M. Han, K. Li, Z. Li, X. Ni, J. Ye, D. Choi, Q. Yang, J. H. Kim, S. Li, S. Chen, C. Wu, D. Lu, J. K. Chang, Z. Xie, Y. Huang, J. A. Rogers, *Sci. Adv.* **2021**, *7*, eabj3686.
[12] R. Xie, W. Zheng, L. Guan, Y. Ai, Q. Liang, R. Xie, W. Zheng, L. Guan, Y. Ai, Q. Liang, *Small* **2020**, *16*, 1902838.
[13] J. H. Bezer, H. Koruk, C. J. Rowlands, J. J. Choi, *Ultrasound Med. Biol.* **2020**, *46*, 3327.
[14] J. Lee, S. H. Lee, B. K. Lee, S. H. Park, Y. S. Cho, Y. Park, *Tissue Eng. Regener Med.* **2018**, *15*, 403.
[15] S. Ma, M. Rong, P. Lin, M. Bao, J. Xie, X. Wang, W. T. S. Huck, F. Zhou, W. Liu, *Chem. Mater.* **2018**, *30*, 6756.
[16] K. Yan, C. Yang, W. Zhong, Z. Lu, X. Li, X. Shi, D. Wang, *Soft Matter* **2020**, *16*, 9471.
[17] X. Zhao, A. Wright, D. E. Goertz, *Ultrason. Sonochem.* **2023**, *93*, 106291.
[18] J. S. Miller, K. R. Stevens, M. T. Yang, B. M. Baker, D. H. T. Nguyen, D. M. Cohen, E. Toro, A. A. Chen, P. A. Galie, X. Yu, R. Chaturvedi, S. N. Bhatia, C. S. Chen, *Nat. Mater.* **2012**, *11*, 768.
[19] M. Ryma, H. Genç, A. Nadernezhad, I. Paulus, D. Schneidereit, O. Friedrich, K. Andelovic, S. Lyer, C. Alexiou, I. Cicha, J. Groll, *Adv. Mater.* **2022**, *34*, 2200653.
[20] T. C. Tseng, F. Y. Hsieh, P. Theato, Y. Wei, S. hui Hsu, *Biomaterials* **2017**, *133*, 20.
[21] L. E. Bertassoni, M. Cecconi, V. Manoharan, M. Nikkhah, J. Hjortnaes, A. L. Cristino, G. Barabaschi, D. Demarchi, M. R. Dokmeci, Y. Yang, A. Khademhosseini, *Lab Chip* **2014**, *14*, 2202.
[22] N. Zhao, Z. Guo, S. Kulkarni, D. Norman, S. Zhang, T. D. Chung, R. F. Nerenberg, R. M. Linville, P. Searson, N. Zhao, Z. Guo, R. M. Linville, P. Searson, S. Kulkarni, T. D. Chung, R. F. Nerenberg, D. Norman, S. Zhang, *Adv. Funct. Mater.* **2022**, *32*, 2110289.
[23] J. Nie, Q. Gao, C. Xie, S. Lv, J. Qiu, Y. Liu, M. Guo, R. Guo, J. Fu, Y. He, *Mater. Horiz.* **2020**, *7*, 82.
[24] H. Yoshida, M. Matsusaki, M. Akashi, *Adv. Funct. Mater.* **2013**, *23*, 1736.
[25] V. K. Lee, D. Y. Kim, H. Ngo, Y. Lee, L. Seo, S. S. Yoo, P. A. Vincent, G. Dai, *Biomaterials* **2014**, *35*, 8092.
[26] K. S. Lim, M. Baptista, S. Moon, T. B. F. Woodfield, J. Rnjak-Kovacina, *Trends Biotechnol.* **2019**, *37*, 1189.
[27] R. Xie, Z. Liang, Y. Ai, W. Zheng, J. Xiong, P. Xu, Y. Liu, M. Ding, J. Gao, J. Wang, Q. Liang, *Nat. Protoc.* **2021**, *16*, 937.
[28] S. A. Williams, S. Wasserman, D. W. Rawlinson, R. I. Kitney, L. H. Smaje, J. E. Tooke, *Clin. Sci.* **1988**, *74*, 507.
[29] K. P. Ivanov, M. K. Kalinina, Y. I. Levkovich, *Microvasc. Res.* **1981**, *22*, 143.
[30] J. H. Spurk, N. Aksel, *Fluid Mechanics*, Springer, New York **2020**.
[31] M. L. Rathod, J. Ahn, N. L. Jeon, J. Lee, *Lab Chip* **2017**, *17*, 2508.
[32] R. Abbasi, T. B. LeFevre, A. D. Benjamin, I. J. Thornton, J. N. Wilking, *Lab Chip* **2021**, *21*, 2050.
[33] H. Yuk, T. Zhang, S. Lin, G. A. Parada, X. Zhao, *Nat. Mater.* **2016**, *15*, 190.
[34] H. Lee, S. M. Dellatore, W. M. Miller, P. B. Messersmith, *Science* **2007**, *318*, 426.
[35] S. E. Park, A. Georgescu, J. M. Oh, K. W. Kwon, D. Huh, *ACS Appl. Mater. Interfaces* **2019**, *11*, 23919.
[36] A. C. Shore, *Br. J. Clin. Pharmacol.* **2000**, *50*, 501.
[37] T. Trantidou, T. Prodromakis, C. Toumazou, *Appl. Surf. Sci.* **2012**, *261*, 43.
[38] S. Haefner, M. Benzaquen, O. Bäumchen, T. Salez, R. Peters, J. D. McGraw, K. Jacobs, E. Raphaël, K. Dalnoki-Veress, *Nat. Commun.* **2015**, *6*, 7409.
[39] R. S. Udan, T. J. Vadakkan, M. E. Dickinson, *Development* **2013**, *140*, 4041.
[40] J. R. Tse, A. J. Engler, *Curr. Protoc. Cell Biol.* **2010**, *47*, 10.
[41] T. F. Sherman, *J. Gen. Physiol.* **1981**, *78*, 431.
[42] S. Ebrahimi, P. Bagchi, *Stem Cells Int.* **2022**, *12*, 4304.
[43] R. Fdhraus, A. Torsten, *Am. J. Physiol.* **1931**, *96*, 562.
[44] P. Gaehtgens, *Biorheology* **1980**, *17*, 183.
[45] M. Czerner, L. S. Fellay, M. P. Suárez, P. M. Frontini, L. A. Fasce, *Procedia Mater. Sci.* **2015**, *8*, 287.
[46] P. Sung-Jin, M. B. Goodman, B. L. Pruitt, in *Conf. Microtechnol. Med. Biol.*, IEEE, Piscataway, NJ **2005**.
[47] N. A. S. Manssor, Z. Radzi, N. A. Yahya, L. M. Yusof, F. Hariri, N. H. Khairuddin, N. H. A. Kasim, J. T. Czernuszka, *Skin Pharmacol. Physiol.* **2016**, *29*, 55.
[48] B. Tavsanli, O. Okay, *Eur. Polym. J.* **2017**, *94*, 185.a
[49] Y.-I. Shen, H. E. Abaci, Y. Krupski, L.-C. Weng, J. A. Burdick, S. Gerecht, *Biomater. Sci.* **2014**, *2*, 655.
[50] C. A. Kienzle-Sterzer, D. Rodriguez-Sanchez, C. Rha, *Makromol. Chem.* **1982**, *183*, 1353.
[51] Y. Wu, Y. Xiang, J. Fang, X. Li, Z. Lin, G. Dai, J. Yin, P. Wei, D. Zhang, *Biosci. Rep.* **2019**,*39*, BSR20181748.
[52] M. Salerno, S. Dante, N. Patra, A. Diaspro, *Microsc. Res. Tech.* **2010**, *73*, 982.